Influence of the SrVO3 thin film thickness integrated on glass thanks to [Ca_2Nb_3O_10]- nanosheets

Marie El Rami, Simon Hurand, Florent Baudouin, Marie Dallocchio, Rosine Coq Germanicus, Alexis Boileau, Sandrine Froissart, Bruno Berini, Ulrike Lüders, Adrian David, et al.

Influence of the $SrVO_3$ thin film thickness integrated on glass thanks to $[Ca_2Nb_3O_{10}]^-$ nanosheets

Marie El Rami[1], Simon Hurand[2], Florent Baudouin[3], Marie Dallocchio[1], Rosine Coq Germanicus[1], Alexis Boileau[1], Sandrine Froissart[1], Bruno Bérini[4], Ulrike Lüders[1], Adrian David[1], Maryline Guilloux-Viry[3], Wilfrid Prellier[1], Yves Dumont[4], Antoine Ruyter[1], Valérie Demange[3], Arnaud Fouchet[1*].

1 Université de Caen Normandie, ENSICAEN, CNRS UMR 6508, CRISMAT, Normandie Univ., 14000 Caen, France

2 Institut Pprime, UPR 3346 CNRS-Université de Poitiers-ENSMA, SP2MI, 86962 Futuroscope-Chasseneuil Cedex, France

3 Univ Rennes, CNRS, ISCR – UMR 6226, ScanMAT – UAR 2025, F-35000 Rennes, France

4 GEMaC, CNRS UMR 8635, Université de Versailles Saint-Quentin-en-Yvelines – Université Paris-Saclay, 45 Av. des États-Unis, 78035 Versailles, France

* Corresponding authors:

E-mail: arnaud.fouchet@ensicaen.fr

Abstract:

Nanosheets (NS) provide an innovative method for growing perovskite thin films on diverse substrates like glass and silicon, serving as germination seeds and offering a cost-effective alternative to expensive monocrystalline substrates. According to the NS transfer process onto the substrate, more than 85-90% of the substrate is covered. However, a small fraction of the perovskite film grows directly on the substrate. This raises several questions: Is the perovskite film grown on glass conductive? How does the NS network influence electrical properties at macroscopic and submicron scales?

To address these questions, we investigated the impact of thickness on the transport properties of transparent conductive $SrVO_3$ vanadate deposited on glass coated with [Ca2Nb3O10]- nanosheets (CNO NS). Macroscopic measurements revealed significant degradation of transport properties at thicknesses below 15 nm. In-plane local electrical properties were examined using Scanning Spreading Resistance Microscopy. Our findings indicate that local transport remains nearly constant when $SrVO_3$ is grown on NS, while a strong thickness dependence is observed when $SrVO_3$ is directly deposited on glass. These results contribute to a better understanding of the growth process, the integration of functional oxides on NS and open new perspectives for tuning the properties of vanadate films as transparent electrodes.

Keywords: vanadates, nanosheets, thickness, local properties

1. Introduction

The use of nanosheets (NS) as seed layers for the growth of thin films is a relatively recent and modern approach. In particular, oxide NS have been suggested to induce crystallinity and control the orientation of complex oxide films [1]. This particular attention to NS is due to their large diversity, cost-effective production, low thickness at the nanometer scale, and their ability to be deposited on any substrate at room temperature and ambient air. For instance, NS have been employed to control the uniaxial orientation of oxide thin films such as ZnO, anatase TiO_2 [1], or perovskite oxides like paramagnetic $SrTiO_3$ [2] , piezoelectric $Pb(Zr_{0.52}Ti_{0.48})O_3$ [3], dielectric $Ba_{1-X}Sr_XTiO_3$ [4], conductive and ferromagnetic $SrRuO_3$ and $La_{0.67}Sr_{0.33}MnO_3$ [5],[6], on glass or silicon, leading to properties comparable to films grown on monocrystalline substrates [4],[7].

In this type of heterostructures, the film exhibits local epitaxy on the NS and a crystallographic texture at the macroscale. However, due to the random in-plane distribution and orientation of the NS when deposited on the substrate, film defects can be introduced such as grain boundaries and/or differences in crystalline qualities between the different film parts: the one deposited on NS and the one directly deposited on glass. The presence of these defects, considered as diffusion centers, could strongly influence the macroscopic transport properties of conductive perovskites [6]. Additionally, the coverage rate of the substrate with the NS is another parameter affecting the electrical properties of the film: a high coverage rate (> 90%) ensures a good percolation between the NS, leading to improved connectivity for the charge carriers and therefore enhancing the conductivity of the textured film grown on top of the NS. Nevertheless, the properties of the perovskite film directly grown on glass, i.e. in the areas that are not covered by NS (< 10%) remain an open question and could significantly influence the overall properties of the thin film.

In this framework, we have chosen $SrVO_3$ (SVO), a well-adapted perovskite, to study this phenomenon since it is a conductor in its crystalline state and can be used as electrode [8]. SVO possesses a cubic perovskite structure with a lattice parameter a = 0.384 nm [9]. This one is close to the 2D in-plane square lattice parameter of $[Ca_2Nb_3O_{10}]^-$ - nanosheets (CNO-NS) (a_{NS} = 0.385 nm) [10], leading to a small lattice mismatch (-0.34%). Not only used as electrode, SVO has recently shown to be a new Transparent Conductor Oxide (TCO) [11],[12],[13] with interesting properties and can be a serious alternative to indium-tin oxide (ITO). SVO is a correlated metal, presenting high carrier concentration (up to 10^{22} cm^3), at least one order of magnitude higher than ITO, which is limited by dopants solubility and self-compensation [14],[15].

Therefore, in this work, we aim to study the influence of the thickness on the electrical conductivity of textured SVO films grown on glass substrates using CNO-NS as template or, at least, as germination centers. According to the macroscopic characterizations (structural and transport properties), the films thickness strongly influences the electronic conduction. Additionally, the role of conductivity of the

vanadate films on NS and bare glass is highlighted by means of advanced electrical atomic force microscope (AFM) measurements in Scanning Spreading Resistance Microscopy (SSRM) mode. This work constitutes a step towards the integration of vanadates with NS in devices and their practical applications.

2. Experimental part:

$[H_{1-y}TBA_y]^+[Ca_2Nb_3O_{10}]^-$ (TBA: TetraButylAmmonium), in what follows noted more simply $[Ca_2Nb_3O_{10}]^-$ (CNO) nanosheets were prepared as described in our previous work [12]. A monolayer of CNO-NS was deposited on two side-polished Eagle XG Corning® glass substrates by unconventional drop casting technique [16]: 120 µL of the CNO solution was diluted into 600 µL of ethanol with 15 mL of ultrapure H_2O. A 70 µL drop of this suspension was loaded with a pipet on the substrate heated at 100°C, and immediately removed by the pipet. The NS covered substrate was then exposed to UV for 30 min, and then set in an oven at 110°C for 1 hour. The coverage rate of the substrate by CNO-NS (Pcoverage) is calculated from the average of five AFM topography scans taken on different parts of each film (see figures S2 and S3 in supplementary information (SI)), with values varying from 86 to 92 %. This value is in accordance with the previous investigations [12], and comparable for all films. SVO thin films were grown on these prepared substrates from a homemade $Sr_2V_2O_7$ target by pulsed laser deposition at 500 °C under base pressure (10^{-6} mbar) to avoid overoxidation of the vanadate phase. Films of SVO with a thickness of 11, 21 and 46 nm were grown. After a previous calibration, a 2 nm thick $LaAlO_3$ (LAO) amorphous protective layer was deposited on the top of the SVO films under the same conditions at 150 °C. The role of this capping layer is to prevent the oxidation of the deposited vanadate films.

Structural properties of SVO thin films were investigated by X-ray diffraction (XRD, Bruker D8 Discover) using Cu $K_{\alpha 1}$ radiation (λ = 1.5406 Å) in Bragg-Brentano configuration with 7s/step and steps of 0.01°, and X-ray reflectometry (XRR) configuration for the thickness measurements. The error calculation of the thickness is detailed and given in the supplementary information.

The resistivity measurements were carried out by means of four-probe technique (*i.e.* macroscopic approach) using a Physical Properties Measurement System designed by Quantum Design. The Van der Pauw configuration was used for all films at 300 K. Hall measurements were conducted in the same temperature range, by applying a magnetic field perpendicular to the sample surface (-9 to 9 T) to determine both the carrier density and mobility.

Electrical properties of the films were also investigated by variable angle spectroscopic ellipsometry (SE), using a J. A. Woollam M2000XI in the UV- to IR- range (UV-vis-NIR) from 0.7 to 5.9 eV (0.211 to 1.700 µm) and a J. A. Woollam IR-Vase Mark II in the IR range from 0.04 to 0.7 eV (1.7 to 40 µm). Measurements were conducted at different incident angles (55°, 65° and 75°) to determine the ellipsometric angles Ψ and Δ. The UV-vis-NIR and IR data were then combined and analyzed concomitantly using the J. A. Woollam Company's Complete EASE software. A pristine glass substrate served as a reference for all measurements.

The films surface morphology was investigated using a Bruker Dimension ICON AFM operating in peak force mode. Additionally, AFM Scanning Spreading Resistance

Microscopy (SSRM) mode was used to probe the submicronic electrical properties. In this experiment, an antimony (n)-doped silicon probe coated with a diamond layer is in strong contact with the sample's examined surface during the measurement process. For this, the probe's spring constant is 42 N/m and the scan rate is 0.5 Hz. In SSRM mode, the local current (at each pixel of the scan) is recorded for a fixed electrical bias of 500 mV DC (see Supplementary Information part 6). This current flows from the conductive tip through the sample to the silver paste side contact. This contact configuration is particularly well adapted to check the in-plane interconnectivity of SVO deposited on CNO-NS or glass. A logarithmic current amplifier is used to determine the total equivalent resistance, which includes the conductive tip resistance, the spreading resistance of the material under the contact, the bulk resistance of the thin film and the CNO-NS (the substrate being insulating), and the side-contact resistance [17],[18].

3. Results and Discussion

Structural properties:

The thickness of the deposited SVO thin films was determined using XRR measurements. The period of the thickness oscillations is varying with the thickness (see figure 1a). The respective thicknesses of the films were determined to be 11 nm, 21 nm and 46 nm by the analysis of the oscillation period. It is important to note that only oscillations attributed to the vanadate layer are perceptible. The amorphous LAO layer and the $[Ca_2Nb_3O_{10}]^-$ - nanosheets (CNO-NS) seed layer are both too thin to exhibit oscillations [12].

The crystalline structure of the films was investigated with XRD in θ-2θ configuration. The patterns are shown in figure 1b. All the films reveal a significant texture in the out-of-plane direction, with only the 001 and 002 reflections present in the limit of detection of the XRD in this configuration[12], [13]. As expected, the intensity of the reflections increases with the film thickness due to a larger interacting volume with the X-rays. The extracted values of the out-of-plane lattice parameters (0.391 nm) are slightly higher than the bulk value (0.384 nm), which can be attributed to a small oxygen or cations off-stoichiometry [19] (see figure S1).

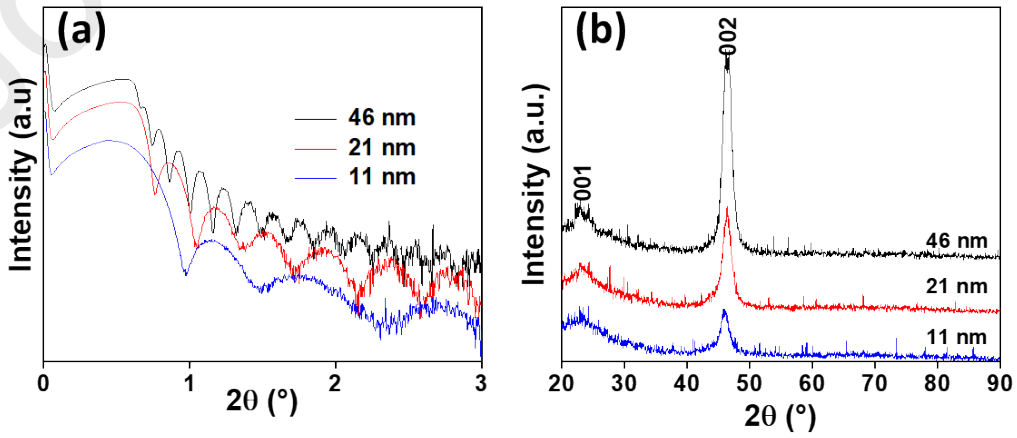

Figure 1: Structural properties of vanadate thin films: (a) XRR of SVO thin films deposited on glass substrates with a CNO-NS seed layer, used to determine the film thickness, (b) θ-2θ XRD patterns of SVO films with different thicknesses.

Macroscopic transport properties:

Two different methods were used and compared to investigate the impact of the film thickness on the transport properties of SVO thin films: direct current (DC) electrical measurements and optical measurements. The latter is based on SE at room temperature, by calculating the complex dielectric function $\varepsilon(\omega) = \varepsilon_1(\omega) + \varepsilon_2(\omega)$. It is important to note that optical measurements examine the free electrons motion at short length scales within the crystalline grains (typically few nanometers at visible wavelengths), whereas DC measurements examine the long-range conductivity throughout the whole film (i.e. film deposited on CNO-NS or directly on glass, grain boundaries,…).

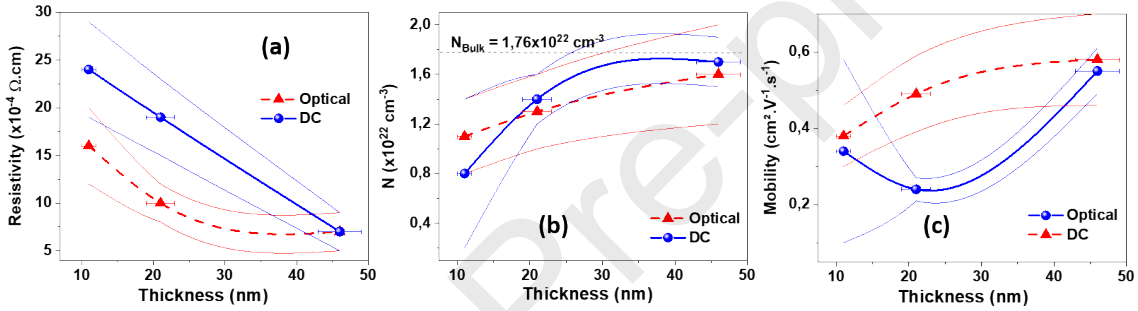

Figure 2: Thickness dependent optical and DC transport properties of vanadate thin films at 300 K. (a) to (c) resistivity, carrier density, and carrier mobility as a function of SVO films thickness ranging from 11 to 46 nm. The red curves represent the values extracted from the SE measurements (optical) and the blue curves refer to the ones calculated from the DC macroscopic measurements. The errors bars are given with the fine lines in red and blue.

The evolution of the macroscopic DC and optical resistivity values at T = 300 K as a function of film thickness is shown in figure 2a. The obtained resistivity values for the 46 nm film coincide very nicely and are coherent with previously reported values on CNO-NS [12],[20], demonstrating the excellent conduction behavior of the SVO thick film. Moreover, these values evidence both negligible grain boundaries scattering as well as a good overall geometrical connectivity between conducting grains even those grown on glass (gaps between NS).

On the contrary, while decreasing the thickness, both measurements reveal an increase of the resistivity, indicating a lower film quality or a poor grain connectivity for thinner films. One possibility of this effect could be the relatively low deposition temperature (500 °C), which can slow down the crystalline ordering dynamics: the

thicker films undergo a longer time at high temperature due to the longer deposition time, hence leading to an improved crystallinity. Another possibility is an increased defect concentration in grains or grain boundaries at lower film thickness. However, the local epitaxial grain-on-NS growth [12] should stabilize high quality crystallization even in very thin films. Thus, the resistivity decrease in our case cannot be only explained by these hypotheses.

Interestingly, the macroscopic DC resistivity (long-range conductivity through the film) increases much more rapidly with decreasing film thickness than the optically derived resistivity (short-length scale). Therefore, we should take into account the “on glass” SVO (referring to SVO grown on uncovered areas with CNO-NS) regions of the film and the grain boundaries, which may have a stronger influence at low thickness compared to the thickest film, where both macroscopic DC and optical resistivity values coincide. The grain boundaries density should remain constant with thickness, considering an almost constant coverage rate. Thus, the observed macroscopic DC resistivity decrease would rather be a sign of a better conduction in the “on glass” SVO regions and in the grain boundaries.

A general increase of the free carrier density N (Figure 2b) and their mobility μ (Figure 2c), is observed with the increase of the film thickness, confirming the higher quality of the thickest film’s grains. Again, the DC values tend to increase more strongly with the film thickness than the optically derived values. Concerning N, both the DC and optical values obtained for the 46 nm thick film are close to the theoretical value of 1.76 x 10^{22} cm^{-3} for one electron per unit cell of SVO [11]. Thus, “on glass” SVO regions seems to be more electrically perturbed for thin films than for thicker ones. As a result, these areas of the film become a source of charge carriers at high film thickness. Both (DC and optical) mobility values measured for the 46 nm thick film are comparable with previous studies [12],[20].

Due to the epitaxial growth of the SVO on the individual CNO-NS and a similar NS coverage rate of the substrate before deposition, these observations rise some questions about the correlation between the film thickness and the influence of the connectivity between the SVO grains. However, based on macroscopic measurements, it is not possible to gain more insights. Therefore, a submicronic analysis of the electrical properties, discriminating between the grain regions, the grain boundary regions, and the film region deposited on areas uncovered by CNO-NS is needed to investigate the variation of the local electrical properties.

Submicronic investigation of transport properties:

Firstly, surface morphologies of the deposited vanadate thin films were determined using AFM microscopy in peak force tapping (scanAsyst) mode. Figure 3 presents the acquired 4 x 4 μm^2 topography images for the different SVO film thicknesses. The lateral size of the NS varies from 100 nm to 1 μm. The thin films were deposited on the glass support covered by CNO-NS, the majority of which are juxtaposed. In some areas of the substrate, a superposition of CNO-NS is observed (bright color in figure 3 a, b and c), caused by the drop casting deposition process. Nevertheless, it should be noted that regardless of the high coverage rate, the sample surface shows areas without CNO-NS, where the film is directly deposited on glass. For each SVO

thickness, namely 11, 21 and 46 nm in figure 3 a-b-c respectively, some profiles from these areas were extracted and reported in figure 3 d-e-f, respectively. For all the different thicknesses, the height difference between these two areas is about 1.4 nm, corresponding roughly to a single CNO-NS thickness (not shown here), showing a conformal film deposition all over the substrate independently of the presence or not of the CNO-NS.

Moreover, these profiles reveal the presence of a thicker region at the nanosheet edge, when located at the CNO-NS/glass border. These bumps are present for all the films and tend to increase with film thickness, from 2 to 6 nm (see profiles in figure 3d-e-f). It is to note that this phenomenon is absent when the CNO-NS are directly adjacent (see figure S8). This suggests that the bump is the result of good wettability of the SVO on the CNO-NS, which leads to an accumulation of material during film growth when an CNO-NS/glass boundary is present. It can be noted that this phenomenon is almost absent when two CNO-NS are side by side. Moreover, if we consider the topography profiles as a function of the thickness of the deposited film, it confirms that the growth of the SVO film is of the layer-by-layer type on CNO-NS and island-like on glass. A comparison of the roughness of the SVO film grown on CNO-NS and SVO directly deposited on glass (see section 5 in SI) shows that the roughness on NS remains constant for the different thicknesses (except at the edge) whereas the roughness of the SVO deposited directly on glass tends to increase with the thickness. This result confirms that “on NS” film growth is a 2D process, allowing for the above considerations about the local epitaxial growth, whereas the growth on glass tends to be a 3D one with an increase of the roughness with the thickness. By considering a 2D growth process on CNO-NS, the edge of nanosheets surrounded with SVO directly on glass, tends to break the layer-by-layer growth and leads to an accumulation of matter, which can play a role in the grain boundary crystallinity.

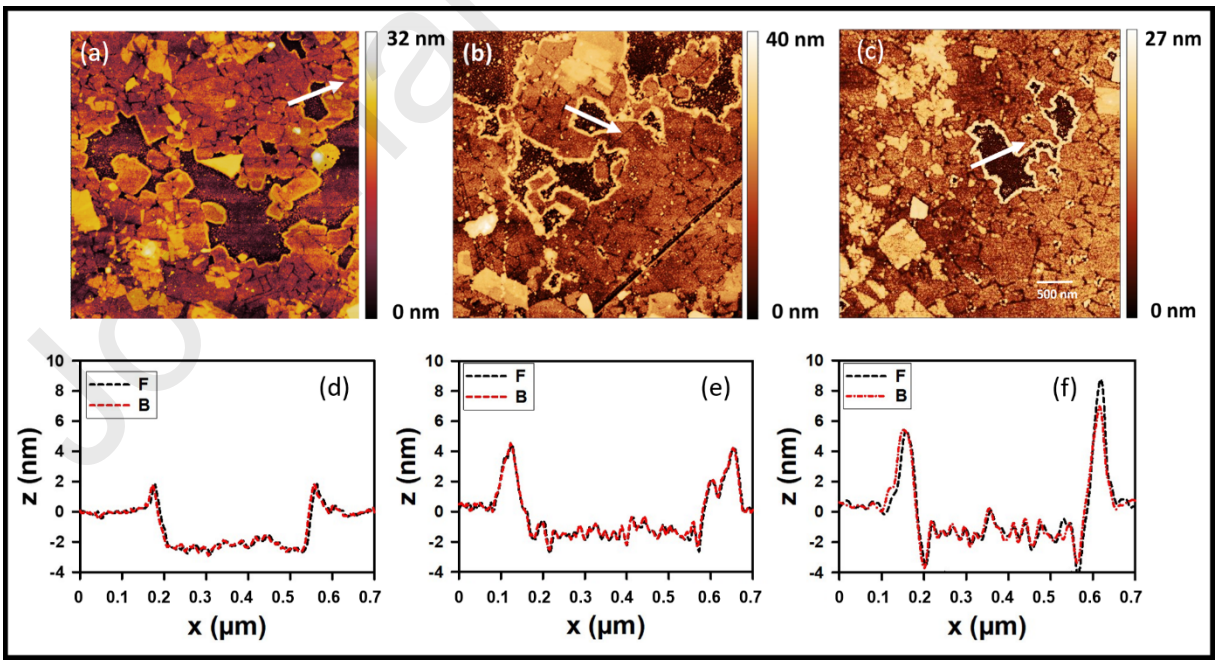

Figure 3: (a), (b) and (c) 4 x 4 µm^2 AFM image of SVO thin films with different thicknesses 11, 21, 46 nm respectively. (d), (e) and (f) are the height profiles extracted from (a), (b) and (c) respectively with the forward scan (F) and backward scan (B), as indicated by the white arrows.

To investigate transport properties, local electrical measurements were conducted using the AFM SSRM mode. This scanning probe microscopy technique uses a conductive probe in contact mode. A 500 mV DC voltage is applied to the tip while scanning, and the sample resistance is then measured through a logarithmic amplifier after two scans to ensure that the LAO insulator capping layer has been removed [21],[22]. In figure 4a and b, the simultaneously recorded topographic and resistance (in logarithmic scale) maps are presented for all films, respectively. A specific focus is made on areas of the film directly grown on glass, noted with mark 2 on the images.

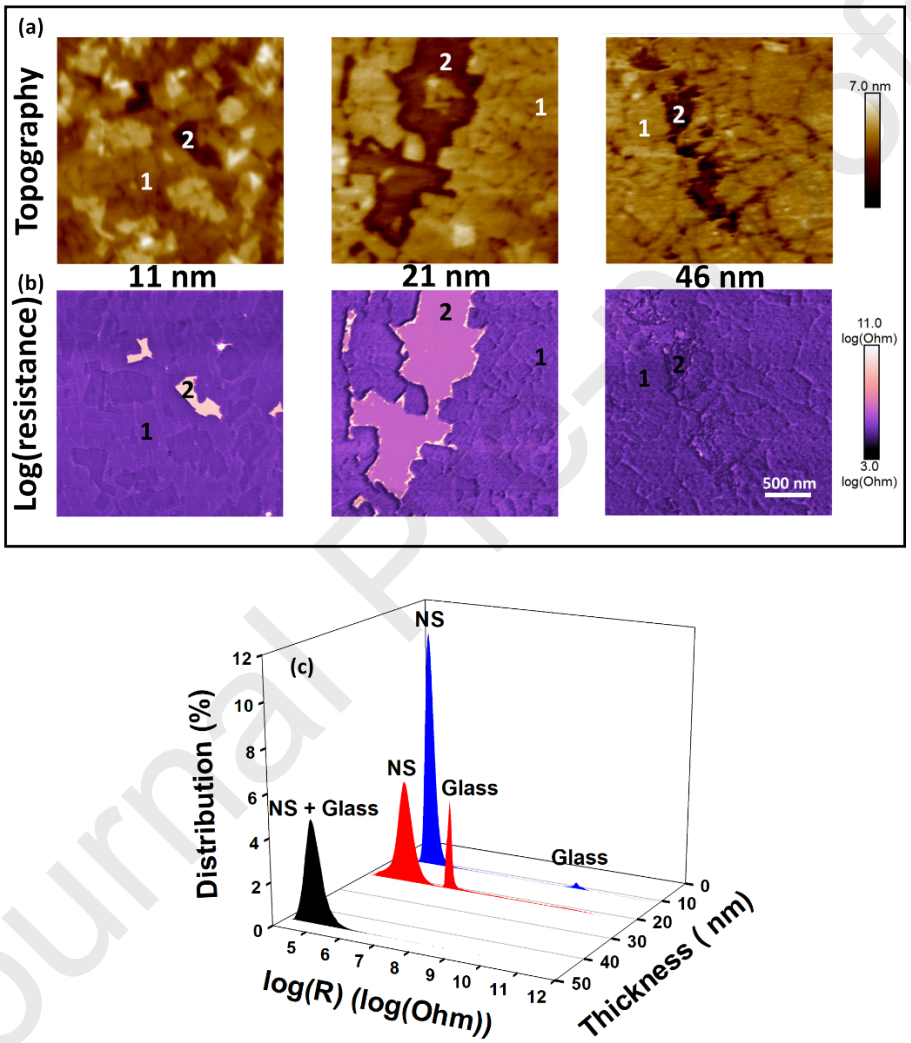

Figure 4: (a) Topography and (b) SSRM maps (2.5 x 2.5 μm^2) on SVO samples with different thicknesses. The numbers on the topography images indicate areas of the film grown on NS (1) and others directly grown on glass (2). (c) Resistance distributions in the scanned areas for the three thicknesses.

Interestingly, for the thinnest films of SVO, ”on glass” areas (2) present much higher resistances than those ”on NS”, while for the thickest film, almost no difference

between the two areas is observed (see figure 4b) indicating that grain boundaries only weakly perturb the electrical transport process.

Furthermore, for each image, the evolution of the resistance distribution for the two different regions were extracted and shown in figure 4c. It displays the mean resistivity values of each area (“on glass” and “on NS”) as a function of the film thickness, together with the resistivity distribution percentage. It must be noticed that a quantitative resistance value is difficult to obtain since with the SSRM technique, a series of resistance is measured, including the contact resistances [17],[18]. Nevertheless, a qualitative analysis reveals that for all the films, the mean resistance value is almost the same for SVO grown on CNO-NS (around 10^5 Ω). This value is consistent with typical SSRM values reported for SVO [17], but even more, it confirms the high quality crystalline growth on the CNO-NS even for the thinnest film. Furthermore, for this thinnest film, the resistance value distribution presents two clear contributions: one corresponding to “on NS” – SVO, and another corresponding to “on glass” – SVO with a difference of five orders of magnitude (black curve in figure 4c). In comparison with the other thicknesses, this analysis shows that the mean resistance of the ”on glass” areas is decreasing with the increase of the film thickness and, finally, merges the “NS” distribution for the thickest film. Therefore, the SVO directly grown on glass presents a strong improvement of the conductivity with thickness, explaining the macroscopic transport measurements.

Such an evolution of electrical properties of the SVO film directly deposited on glass might be an indicator of the crystalline state of SVO for the thickest films, as this material is not conducting in the amorphous state [23]. The observed decrease of the resistivity with the film thickness for the “on-glass” areas should translate therefore an evolution from an amorphous or conductive isolated islands to a continuous crystalline SVO phase. The 3D growth process observed in these areas underlines the spontaneous crystallization process, i.e. without structural template, which is known to be thermodynamically more complicated than epitaxial crystallization using a growth template. Therefore, we can expect that the increase of the film thickness leads to the presence of crystalline seeds which are at the origin of a 3D crystallization process for SVO directly deposited on glass as shown in SI (see section 5). When the film thickness is increased from 11 to 21 nm, the “on glass” – SVO can no more be considered as insulator but still exhibits a higher resistivity value compare to “on NS” – SVO. These results confirm that, for 21 nm, the crystallization process has already started and that the SVO islands are all connected to each other through resistive grain boundaries. The “on glass” – SVO crystallization process is confirmed for the thickest film (46 nm) when the resistivity is almost homogenous independently of the substrate. Furthermore, the weak SSRM contrast at grain boundaries confirms good quality electrical interconnectivity between “on NS” – SVO grains and “on glass” – ones. In the case of 11 nm thick films, grown at a temperature only slightly higher than the crystallization temperature threshold [12], the thermal energy and the available matter are not enough to form stable, long range crystalline seeds for the film crystallization.

This electrical change of the “on glass” – SVO regions, with varying thickness can also be interpreted within the framework of a random network of resistances which can provide a quantitative analysis of the transport properties. The thickness dependence of the local electrical response for SVO regions directly deposited on glass can be used to understand the discrepancies between transport measurements (ρ_{DC}) and optical

measurements (ρ_{Opt}). As explained in the supplementary information of reference [12], the simplified Bruggeman model (Effective Medium Approximation, EMA) describes a network of 2D resistors. Using this model and by comparing optical and DC resistivity values, we can evaluate the connectivity of the crystalline network. In this model, the theoretical DC resistivity ρ_{DC} can be calculated from the resistivity of the crystallized phase ρ_{DC}^{Cryst}, by taking into account the fraction of the crystallized phase *f* of the film and the inter-grain connectivity *L* [24] :

$$\rho_{DC} = \rho_{DC}^{Cryst} \frac{1-L}{f-L} \quad (Eq.\ 1)$$

L takes a value of 0 for perfect electronic transport between the grains, and 1 in the case of absence of electronic transport. The value of *f* is given by the experimental NS coverage rate from the AFM measurements (Supporting Information).

First, we analyzed the SVO film with a thickness of 11 nm. Indeed, the results obtained by near-field microscopy (SSRM) have clearly highlighted that, for such a SVO thickness, two phases co-exist: a conductive one ("on NS" – SVO) and an insulating one ("on glass" – SVO). The analysis of the inter-grain connectivity *L* may therefore reflect the change of the resistances of the SVO layer grown on glass. As seen in figure 4 c (black curve), the difference between resistance values of these two co-existing phases is 5 orders of magnitude. Therefore, "on glass" SVO film can be approximated as not participating to the transport. In this case, we have two extreme resistance values allowing correct analysis using the EMA approach. In addition, for the 11 nm thick film, an intermediate connectivity is considered and L should be around ≈ 0.50 (figure S43 in supplementary information of reference [12]). By considering a negligible grain boundary scattering ($\rho_{DC}^{Cryst} = \rho_{opt}$) and considering the coverage rate (see table S1 in SI), we can estimate the depolarization factor from equation 1 which can be estimated as L= 0.66 for 11 nm.

Regarding the intermediate SVO film thickness (21 nm), SSRM analysis reveals that "on glass" parts of the film are not insulators, but are only less conductive than "on NS" ones with a resistance difference of 2 orders of magnitude (red curve in figure 4 c). Therefore, an analysis using EMA approach is not possible.

It is important to note that above a critical thickness of SVO (21 nm < $t_{SVO}^{Threshold}$ < 46 nm), we no longer observe a bimodal distribution of the resistances measured by SSRM. Therefore, for t_{SVO} = 46 nm, the contributions of the different SVO grains ("on glass" and "on NS") to the resistivity are almost equivalent and allow us to consider a fraction of the crystallized phase almost equal (*f* ≈ 1) for conductive grains. Considering that both DC and optical resistivity measurement lead to the same value ($\rho_{opt} \approx \rho_{DC}$), we can conclude that the connectivity is almost perfect (L ≈ 0) and that the role of the grain boundaries is negligible for "on glass" – 3D crystallized SVO and t_{SVO} larger than $t_{SVO}^{Threshold}$. This indicates very robust conduction in the SVO TCOs, allowing for low resistivity textured films.

Finally, the crystallization process of SVO directly on glass between the CVO-NS raises some questions and opens perspectives. Specifically, it would be interesting to examine and understand the mechanisms underlying the crystallization of the SVO directly on glass, whether it is induced by the proximity with the nanosheets used as a

seed layers [25] or is simply onset by the increase of thickness. For this, we conducted deposition of SVO directly on glass with different thicknesses (see Supplementary Information part 7). We also observed a 3D growth directly on glass with the SVO thickness and an increase of the resistivity when the thickness decreases confirming our first conclusions. Interestingly we can also conclude that the increase of thickness induces a spontaneous crystallization of the SVO with always a higher resistivity compare to the SVO on-NS for the same thickness, showing the importance of the nanosheet as seed layer. This approach is different compare to the one proposed by Taira et *al*. [25] , here we focused on one step SVO growth at low temperature (500 °C) with high NS coverage (90%) more adapted for industrial constrains. Moreover, the results obtained at the submicron scale clearly highlight the importance of optimizing the coverage rate (ideally 100%) in order to improve the electrical properties of SVO films deposit on CNO-NS.

Conclusions

In conclusion, the nanosheets (NS) approach is a reliable method for producing high-quality textured SVO films and opens a new perspective for the practical applications of this material as Transparent Conducting Oxide, especially in Complementary Metal Oxide Semiconductor based devices. Nevertheless, the electrical properties are strongly dependent on the SVO thickness, particularly impacted by the small fraction of the SVO film directly deposited on glass. For a film thickness of 11 nm, film areas deposited directly on glass show an almost insulating character. As the film thickness increases, the resistivity decreases due to the onset of “on glass” crystallization, leading to an improved connectivity between the SVO grains deposited on NS covered substrate areas, as demonstrated by the local electrical properties probed by AFM SSRM. A bimodal SSRM resistances distribution appears for thinner films. As the thickness is increased, these two distribution peaks merge in a centered distribution for SVO thickness between 21 and 46 nm. Three different techniques were used to explain transport properties: optical techniques, sensitive to the intra-grain properties, DC techniques, sensitive to the transport in grain boundaries or other perturbed areas, and SSRM ones. This last approach allows us to clearly identify local electrical properties and, combined with the two others, to disentangle even quantitatively the different contributions, and highlight the specific resistance behavior of the “on glass” – SVO film. These results can be also very useful to improve the physical properties of the textured films. If a higher coverage percentage (ideally 100 %) is achieved either by optimizing the conditions during the drop casting process or by using another nanosheets deposition technique, it would be possible to use ultra-thin films without suffering from a degradation of the transport properties. On the other hand, a much smaller coverage rate could be used for film thickness around or above 40 nm again avoiding the degradation of the transport properties.

Acknowledgements

The authors acknowledge the French Agence Nationale de la Recherche (ANR) (ANR-23-CE08-0008) in the framework of the DisTCOvery project for financial support. The authors have a thought for S. Froissard who recently passed away. They thank her for her involvement in this work and, above all, for her friendliness, which will be missed by all.

References

[1] T. Shibata, K. Fukuda, Y. Ebina, T. Kogure, T. Sasaki, One-nanometer-thick seed layer of unilamellar nanosheets promotes oriented growth of oxide crystal films, Advanced Materials 20 (2008) 231–235. https://doi.org/10.1002/adma.200701381.

[2] T. Shibata, H. Takano, Y. Ebina, D.S. Kim, T.C. Ozawa, K. Akatsuka, T. Ohnishi, K. Takada, T. Kogure, T. Sasaki, Versatile van der Waals epitaxy-like growth of crystal films using two-dimensional nanosheets as a seed layer: Orientation tuning of SrTiO3 films along three important axes on glass substrates, Journal of Materials Chemistry C 2 (2014) 441–449. https://doi.org/10.1039/c3tc31787k.

[3] M.D. Nguyen, H. Yuan, E.P. Houwman, M. Dekkers, G. Koster, J.E. Ten Elshof, G. Rijnders, Highly Oriented Growth of Piezoelectric Thin Films on Silicon Using Two-Dimensional Nanosheets as Growth Template Layer, ACS Applied Materials and Interfaces 8 (2016) 31120–31127. https://doi.org/10.1021/acsami.6b09470.

[4] C. Jung, T. Ohnishi, M. Osada, K. Takada, T. Sasaki, Oriented Film Growth of Ba1−xSrxTiO3 Dielectrics on Glass Substrates Using 2D Nanosheet Seed Layer, ACS Applied Materials & Interfaces 5(11) (2013) 4592–4596.

[5] M. Nijland, S. Kumar, R. Lubbers, D.H.A. Blank, G. Rijnders, G. Koster, J.E. Ten Elshof, Local control over nucleation of epitaxial thin films by seed layers of inorganic nanosheets, ACS Applied Materials and Interfaces 6 (2014) 2777–2785. https://doi.org/10.1021/am4052624.

[6] A. Boileau, M. Dallocchio, F. Baudouin, A. David, U. Lüders, B. Mercey, A. Pautrat, V. Demange, M. Guilloux-Viry, W. Prellier, A. Fouchet, Textured Manganite Films Anywhere, ACS Applied Materials and Interfaces 11 (2019) 37302–37312. https://doi.org/10.1021/acsami.9b12209.

[7] K. Kikuta, K. Noda, S. Okumura, T. Yamaguchi, S.I. Hirano, Orientation control of perovskite thin films on glass substrates by the application of a seed layer prepared from oxide nanosheets, Journal of Sol-Gel Science and Technology 42 (2007) 381–387. https://doi.org/10.1007/s10971-006-0200-z.

[8] Y. Bourlier, M. Frégnaux, B. Bérini, A. Fouchet, Y. Dumont, D. Aureau, XPS monitoring of SrVO3 thin films from demixing to air ageing: The asset of treatment in water, Applied Surface Science 553 (2021). https://doi.org/10.1016/j.apsusc.2021.149536.

[9] M.J. Rey, P. Dehaudt, J.C. Joubert, B. Lambert-Andron, M. Cyrot, F. Cyrot-Lackmann, Preparation and structure of the compounds SrVO3 and Sr2VO4, Journal of Solid State Chemistry 86 (1990) 101–108. https://doi.org/10.1016/0022-4596(90)90119-I.

[10] F. Baudouin, V. Demange, S. Ollivier, L. Rault, A.S. Brito, A.S. Maia, F. Gouttefangeas, V. Bouquet, S. Députier, B. Bérini, A. Fouchet, M. Guilloux-Viry, Orientation control of KNbO3 film grown on glass substrates by Ca2Nb3O10− nanosheets seed layer, Thin Solid Films (2019). https://doi.org/10.1016/j.tsf.2019.137682.

[11] L. Zhang, Y. Zhou, L. Guo, W. Zhao, A. Barnes, H.T. Zhang, C. Eaton, Y. Zheng, M. Brahlek, H.F. Haneef, N.J. Podraza, M.H.W. Chan, V. Gopalan, K.M. Rabe, R. Engel-Herbert, Correlated metals as transparent conductors, Nature Materials 15 (2016) 204–210. https://doi.org/10.1038/nmat4493.

[12] A. Boileau, S. Hurand, F. Baudouin, U. Lüders, M. Dallocchio, B. Bérini, A. Cheikh, A. David, F. Paumier, T. Girardeau, P. Marie, C. Labbé, J. Cardin, D. Aureau, M. Frégnaux, M. Guilloux-Viry, W. Prellier, Y. Dumont, V. Demange, A. Fouchet, Highly Transparent and Conductive Indium-Free Vanadates Crystallized at Reduced Temperature on Glass Using a 2D Transparent Nanosheet Seed Layer, Advanced Functional Materials 32 (2022). https://doi.org/10.1002/adfm.202108047.

[13] P.T.P. Le, S. Ni, P.A. Repecaud, E. van der Minne, K.J.H. Van Den Nieuwenhuijzen, M.D. Nguyen, J.E. ten Elshof, M. Morales-Masis, G. Koster, Correlated Metals Transparent Conductors with High UV to Visible Transparency on Amorphous Substrates, Advanced Materials Interfaces 2201335 (2022) 1–8. https://doi.org/10.1002/admi.202201335.

[14] K. Ellmer, A. Klein, ZnO and its applications, Springer Series in Materials Science 104 (2008) 1–33. https://doi.org/10.1007/978-3-540-73612-7_1.

[15] A. Janotti, C.G. Van De Walle, Native point defects in ZnO, Physical Review B - Condensed Matter and Materials Physics 76 (2007) 1–22. https://doi.org/10.1103/PhysRevB.76.165202.

[16] Y. Shi, M. Osada, Y. Ebina, T. Sasaki, Single droplet assembly for two-dimensional nanosheet tiling, ACS Nano 14 (2020) 15216–15226. https://doi.org/10.1021/acsnano.0c05434.

[17] R.C. Germanicus, Y. Bourlier, V. Notot, B. Bérini, V. Demange, M. Berthe, A. Boileau, M. Euchin, Y. Dumont, D. Aureau, M. Fregnaux, B. Grandidier, U. Lüders, A. David, W. Prellier, L. Biadala, A. Fouchet, Three dimensional resistance mapping of self-organized Sr3V2O8 nanorods on metallic perovskite SrVO3 matrix, Applied Surface Science 510 (2020) 145522. https://doi.org/10.1016/j.apsusc.2020.145522.

[18] R. Coq Germanicus, P. Leclère, Y. Guhel, B. Boudart, A.D. Touboul, P. Descamps, E. Hug, P. Eyben, On the effects of a pressure induced amorphous silicon layer on consecutive spreading resistance microscopy scans of doped silicon, Journal of Applied Physics 117 (2015). https://doi.org/10.1063/1.4923052.

[19] J.A. Moyer, C. Eaton, R. Engel-Herbert, Highly conductive SrVO3 as a bottom electrode for functional perovskite oxides, Advanced Materials 25 (2013) 3578–3582. https://doi.org/10.1002/adma.201300900.

[20] P. Tran, P. Le, S. Ni, P. Repecaud, E. Van Der Minne, K.J.H. Van Den Nieuwenhuijzen, M.D. Nguyen, J.E. Elshof, M. Morales-masis, G. Koster, Correlated Metals Transparent Conductors with High UV to Visible Transparency on Amorphous Substrates, Advanced Materials Interfaces 2201335 (2022) 1–8. https://doi.org/10.1002/admi.202201335.

[21] P. Eyben, S. Denis, T. Clarysse, W. Vandervorst, Progress towards a physical contact model for scanning spreading resistance microscopy, Materials Science and Engineering B: Solid-State Materials for Advanced Technology 102 (2003) 132–137. https://doi.org/10.1016/S0921-5107(03)00019-9.

[22] W. Vandervorst, C. Fleischmann, J. Bogdanowicz, A. Franquet, U. Celano, K. Paredis, A. Budrevich, Dopant, composition and carrier profiling for 3D structures, Materials Science in Semiconductor Processing 62 (2017) 31–48. https://doi.org/10.1016/j.mssp.2016.10.029.

[23] P. Marie, A. Boileau, A. Cheikh, A. Fouchet, A. David, C. Labb, Optical and electrical properties of the transparent conductor SrVO 3 without long-range crystalline order, Applied Physics Letters 112 (2018) 021905.

[24] D.A.G. Bruggeman, The calculation of various physical constants of heterogeneous substances. I. The dielectric constants and conductivities of mixtures composed of isotropic substances., Annals of Physics 416 (1935) 636–791.

[25] K. Taira, Y. Hirose, S. Nakao, N. Yamada, T. Kogure, T. Shibata, T. Sasaki, T. Hasegawa, Lateral Solid-Phase Epitaxy of Oxide Thin Films on Glass Substrate Seeded with Oxide Nanosheets, ACS Nano 8 (2014) 6145–6150. https://doi.org/10.1021/nn501563j.

Highlights

- One Step Integration of $SrVO_3$ on glass with CNO nanosheets
- Evidence for a 2D growth mechanism of SVO on nanosheet seed layers
- Thickness effect on electron conductivity properties
- Thickness dependence of the local conductivity of $SrVO_3$ films determined by SSRM Scanning Probe Microscopy